An Unlimited Color Palette from Perylene Derivative Molecules Dispersed within Hybrids

Yixuan Guo, Damien Boyer, François Reveret, Federico Cisnetti, Geneviève Chadeyron, Fabrice Leroux, Yongjun Feng

An Unlimited Color Palette from Perylene Derivative Molecules Dispersed within Hybrids

Yixuan Guo[a], *Damien Boyer**[,b], *François Reveret*[b], *Federico Cisnetti*[b], *Geneviève Chadeyron*[b], *Fabrice Leroux**[,b], *Yongjun Feng**[,a]

[a] State Key Laboratory of Chemical Resource Engineering, Beijing Engineering Center for Hierarchical Catalysts, Beijing University of Chemical Technology, No. 15 Beisanhuan East Road, Beijing 100029, China

[b] Université Clermont Auvergne, Clermont Auvergne INP, CNRS, ICCF, F-63000 Clermont-Ferrand, France

*Emails: damien.boyer@sigma-clermont.fr (DB); fabrice.leroux@uca.fr (FL); yjfeng@mail.buct.edu.cn (YF)

ABSTRACT: Subject to the aggregation-caused quenching (ACQ) mechanism in the solid state, perylene and its derivatives turn to be fascinating organic fluorophores when separated from each other by their co-intercalation within a layered double hydroxide host structure. Such accommodation with surfactant spacers limits their stacking usually caused by π-π interaction between neighboring cores. For each series of fluorophores having substitution in *bay* or diimide positions, an optimized composition is selected based on optical performances and in particular on the absolute photoluminescence quantum yield. The optimal relative quantity of phosphor is very

low from 0.001 to 0.1 % of the total anionic capacity. When dispersed into silicone matrix, the loaded films cover from green (510 nm) to red (625 nm) emission depending on the perylene derivative molecules. With loaded films overlaid on a blue chip, a warm white light (CCT = 3890 K) with a color rendering index (CRI) as high as 91.1 is reached. In such a LED configuration, the superposition of films for each fluorophore is preferred to the powder mixture or to the co-intercalation of organic phosphors within the same structure in order to avoid too strong and non-predictable re-absorption phenomena between emitting centers.

KEYWORDS: Perylene derivatives, organic phosphors, layered double hydroxides, tunable color polysiloxane composite films, LED display

1. INTRODUCTION

The development of light-emitting materials is a growing research area for optoelectronic and photonic devices.[1-4] Perylene and its derivatives (PD), an appealing class of polycyclic aromatic chromophores, are well-known to possess outstanding photophysical characteristics such as an excellent photoluminescence quantum yield (PLQY), a high absorption coefficient, a wide color emission, as well as high chemical, thermal and photo-stabilities. Moreover, they have already been studied as photoluminescent materials.[5,6] Hence, they have recently received extensive attention for their use as an advanced optical-functional material for applications in light-emitting diodes (LEDs), chemo-sensors, field-effect transistors, and solar cells.[7-9] One the other hand, a major and blocking critical point for their use is their very strong affinity to pile up and in fact to lose their optical properties in the solid state or in concentrated solutions.[10] Indeed, the conjugated perylene cores exhibit a strong tendency towards intermolecular π-π stacking, leading to

aggregates.[11] The photoluminescence quantum efficiency decreases with concentration increasing since the formation of π-π stacked aggregates results in energy loss through a non-radiative pathway. This phenomenon called "aggregation-caused quenching" (ACQ) is well-known for π-conjugated systems.[12] Most of perylene-based solids are commonly non-fluorescent owing to the ACQ effect, even in solution because they are hydrophobic in polar solvents and tend to aggregate. Since solid state luminescence is essential to be able to build optical devices, many efforts are devoted to prevent π-π interactions between perylene-based backbones.

One approach is to introduce covalently bulky substituents at the *bay*-, imide- and/or ortho-position to suppress aggregation.[13] It should be noticed that the substitution at *bay* position twists the perylene-based planar conformation usually more than a substitution at the imide position.[14,15] Molecular insulation is another effective strategy to disrupt stacking by incorporating PD phosphors into films or supramolecular assemblies such as poly(ethylene glycol) (PEG), polyglycerol (PG) dendrons, and dendritic carbohydrate derivatives. Such soft matters wrap PD molecules and obstruct their perylene core aggregation.[16,17] These two above-mentioned methods effectively limit interactions by π-π stacking between perylene backbones, however, for the former their structural design requires complicated organic synthetic steps while soft matters are usually thermally unstable. Therefore, functionalized and stabilized PD materials exhibiting excellent photoluminescence performance in solid state are still awaited.

Alternatively, an elegant approach is to protect and disperse the organic fluorophores within a host structure such as metal-organic frameworks (MOFs) or 2D layered structures.[18-20] As expected, interactions between organic guests and the host modify the degree of stacking and aggregation of the fluorescent molecules. MOFs exhibit stable cages capable of accommodating organic molecules and thus inhibiting the ACQ effect by metal-ligand coordination interactions.[21-

[23] Otherwise, as another inorganic framework of interest, layered double hydroxides (LDHs) received a lot of attention since they can be easily combined with photoactive organic molecules.[24,25] Widely tunable in compositions and easy to synthesize, LDHs are composed of a positively charged brucite-like layer in the host sheet and negatively intercalated guest anions in the interlayer region as well as water molecules, and generally described with the chemical formula $[M^{2+}_{1-x}M^{3+}_{x}(OH)_2](A^{n-}_{x/n})\cdot mH_2O$ (M^{2+} and M^{3+}: di- and tri-valent metal ions, respectively, A^{n-}: guest anions).[26,27] The LDH materials have many benefits: (1) rigid layers providing a stable and protective structure, (2) immobilization and dispersion of phosphors in a confined environment, thus preventing the PD molecules from piling up between them, and (3) a good state of dispersion in a polymer medium by surface modification.[28,29] Thus, the LDH host structure is an ideal platform to prevent π-stacking between aromatic fluorophores in the solid state and as functional polymer fillers in the idea of manufacturing solid-state white LEDs.[30] In addition, in order to avoid interactions between guest species as much as possible, which causes emission to stop, the content of PD phosphors must be very low. Indeed, due to the dense molecular packing provided by the LDH exchange material, the fluorescent molecules must be further dispersed by co-intercalation with non-photoactive molecules such as surfactant molecules. Usually, long alkyl chain surfactants are preferred such as dodecylsulfate (DS) or dodecylbenzenesulfonate (DBS) since they space the layers and allow the phosphors to be well accommodated and ensconced within the LDH galleries.[31-34]

In this article, four water-soluble molecules are synthesized from a perylene core and co-intercalated in the interlamellar space of Mg_2Al-LDH with surfactant molecules (DS) by co-precipitation. Schematic 1 shows the synthetic routes of four fluorophores and the corresponding synthesis details are described in Supporting Information. For each series of $DS_{1-ax}PD_x^{a-}$-LDH

inorganic-organic hybrid materials, the dispersion degree of PD guests is finely optimized by tuning the molar ratio *x* between the interlayer guests that modulates the phenomenon of absorption and emission for the whole solid. The structural and optical characterizations of the different series DS-PD$_x$-LDH are investigated using XRD, FT-IR, and UV-vis as well as photoluminescence spectroscopy. The optimized compositions of DS-PD$_x$-LDH powders were dispersed in a silicone matrix in the required proportions to minimize aggregation and lead to luminescent composite films with the best optical performance. Placed on a commercial blue LED chip to produce warm white light, the films emitting different colors are overlaid and the photometric parameters (color rendering index (CRI), color correlated temperature (CCT) and chromaticity coordinates) are recorded. In addition to this classic way of using a single organic fluorophore intercalated in a single LDH structure per film, two other approaches are tested: the physical mixing of the optimized DS-PD$_x$-LDH powders in the same polysiloxane film, as well as the intercalation of the phosphors in the same LDH structure and dispersed in a single film. Depending on the configuration chosen, different results are recorded, notably due to re-absorption phenomena between films, or between mixed powders, or between co-intercalated phosphors that must be avoided as much as possible to obtain quality light performance or that must be mastered in order to judiciously control the color of light emission.

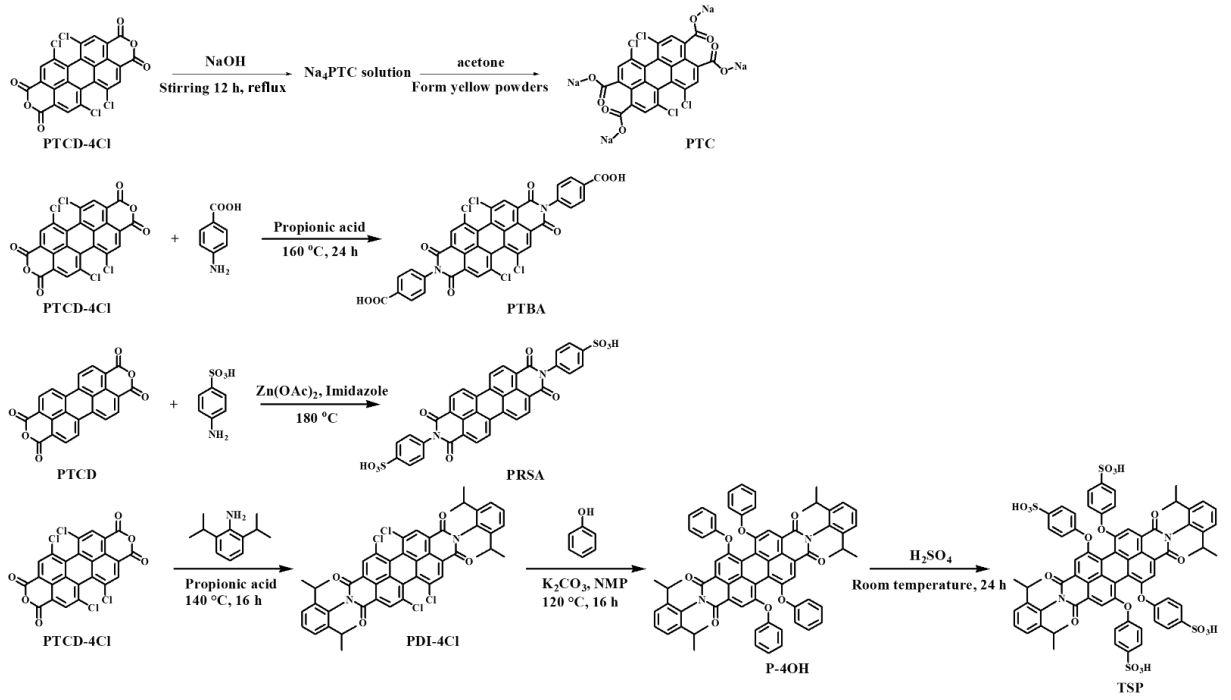

Schematic 1. Synthetic routes of the sodium salt of 1, 6, 7, 12-tetrachloroperylene-3, 4, 9, 10-tetracarboxylic acid dianhydride (PTC), N,N'-di-(4-benzoic acid)-1, 2, 6, 7-tetrachloroperylene-3, 4, 9, 10-tetracarboxylic acid diimide (PTBA), N,N′-bis(4-benzenesulfonic acid)perylene-3,4,9,10-tetracarboxylic acid diimide (PRSA) and N,N′-bis(2,6-diisopropylphenyl)-1,6,7,12-tetra-(4-sulfophenoxy)perylene-3,4,9,10-tetracarboxydiimide (TSP).

2. EXPERIMENTAL SECTION

2.1. Chemicals

All the reagents were purchased from commercial sources and used without further purification. 1,6,7,8-tetrachloroperylene-3,4,9,10-tetracarboxylic acid dianhydride (PTCD-4Cl, 96 %) and perylene-3,4,9,10-tetracarboxylic acid dianhydride (PTCD, 98 %) was obtained from Aladdin. Propionic acid (99.5 %), para-aminobenzoic acid (99%), *N*,*N*-dimethylformamide (DMF, 99.8 %), sulphanilic acid (99 %), imidazole (99 %), phenol (99 %), dichloromethane (DCM, 99.8 %), 2,6-diisopropylaniline (97 %), and *N*-methylpyrrolidone (NMP, 99 %) were provided by Acros-organics. Acetone (99.9%), methanol (99.5 %), ethanol (99.5 %), zinc acetate (99.9 %),

magnesium nitrate hexahydrate ($Mg(NO_3)_2 \cdot 6H_2O$, 99.9 %), aluminum nitrate nonahydrate ($Al(NO_3)_3 \cdot 9H_2O$, 99.9 %), sodium hydroxide (NaOH, 97 %), sodium dodecylsulfate ($CH_3(CH_2)_{11}SO_4Na$, 98.5 %), concentrated sulfuric acid (H_2SO_4, 98 %), anhydrous potassium carbonate (K_2CO_3, 99.9 %), and concentrated hydrochloric acid (HCl, 37 %) were purchased from Sigma-Aldrich. Additionally, the two-component polysiloxane, Bluesil™ RTV 141 A&B, was supplied by Bluestar Silicones (now Elkem).

2.2. Synthesis of DS-PD$_x$-LDH nanofillers

The synthetic procedures of the four perylene derivatives (PD) are shown in Supporting Information. They were co-intercalated with dodecyl sulfonate (DS) into the interlayer galleries of LDH by a one-step co-precipitation thus defining the entire series of general composition $DS_{1-nx}PD_x^{n-}$-LDH as a function of the percent of PD molecules (Figure 1b, labeled as DS-PTC$_x$-LDH, DS-PTBA$_x$-LDH, DS-PRSA$_x$-LDH and DS-TSP$_x$-LDH, respectively). For instance, for DS-PTC$_x$-LDH, 0.51 g of $Mg(NO_3)_2 \cdot 6H_2O$ (2.00 mmol) and 0.38 g of $Al(NO_3)_3 \cdot 9H_2O$ (1.00 mmol) were dissolved in 50 mL of deionized water as solution A, 0.24 g of NaOH (6 mmol) was dissolved in 50 mL of deionized water as solution B, and solution C is a 50 mL of aqueous solution containing DS (a mmol) and PTC (b mmol, its corresponding *x* value refers to the feeding molar ratio of PTC/(SDS+PTC) with the formula of x (%) = b/(a + b) × 100 (%) and a + 4b = n (Al^{3+})). The solution A was added dropwise into solution C with a rate of 0.4 mL/min at room temperature under N_2, and the pH kept at 9.5-10 using solution B. Then, the mixture was aged with stirring overnight at room temperature under N_2. The final yellowish-green powder was centrifuged and washed several times with deionized water, and dried at 40 °C for 24 h. DS-PTBA$_x$-LDH, DS-PRSA$_x$-LDH and DS-TSP$_x$-LDH were synthesized in a similar procedure. It is worth noting that,

for DS-PTBA$_x$-LDH and DS-PRSA$_x$-LDH, the x value was calculated from x (%) = b/(a + b) × 100 % with a + 2b = n (Al^{3+}). For DS-PTBA$_x$-LDH, it was required to add PTBA in 10 mL of NaOH aqueous solution with pH 9.5-10 ahead of schedule under stirring for 2 h to guarantee it dissolved completely in view of its insolubility in water. The feeding concentration of PD molecules in the four series of DS-PD$_x$-LDH samples is listed in Table S1 (Supporting Information).

2.3. Fabrication of polysiloxane/PD-LDH composite films

The two-component polysiloxane (Bluesil^{TM} RTV 141 A&B) was composed of a viscous liquid (part A, 90 wt.%), cured by polyaddition reaction with a catalyst (part B, 10 wt.%). All the DS-PD$_x$-LDH powders were dispersed in silicone matrix at different loadings. Typically, a 40 wt.% PTC$_{0.1}$-LDH composite film (labeled as Si/PTC-LDH) was prepared as follows: a mixture of 1.62 g of part A and 1.2 g of PTC$_{0.1}$-LDH were dispersed in a mechanical mixer (Planetary Centrifugal Vacuum Mixer "Thinky Mixer") at 1200 rpm for 10 min then homogenized by being pressed twice through a three-roller mill (Exakt80E). 0.18 g of part B was then added to the mixture and further homogenized using the mechanical mixer for 10 min at 1200 rpm. Finally, the polysiloxane/filler composite film was casted onto a Teflon surface called Elcometer 4340 automatic film applicator at 40 °C (the knife blade height was 200 μm and the casting speed was 30 mm/s) then curing at 70 °C for another 2 h. The film thickness was measured with an Elcometer 456 coating thickness gauge. Similarly, polysiloxane/PTBA$_{0.05}$-LDH (40 wt.%), polysiloxane/PRSA$_{0.05}$-LDH (40 wt.%), and polysiloxane/TSP$_{0.1}$-LDH (5, 10, 15, 20, 40 wt.%) films were prepared in the same way.

2.4. Characterization

X-Ray Diffraction measurements of PD, DS-PD$_x$-LDH powders, and Si/PD-LDH composite films were performed on a Philips X'Pert Pro diffractometer using Cu Kα radiation (λ = 1.54 Å). The patterns were collected in a 2θ range from 2 to 70° with a step size of $1^{o}min^{-1}$. Fourier transform infrared (FT-IR) spectroscopy were recorded with a Thermo-Nicolet 5700 FT-IR spectrometer equipped with transmission mode. The data were obtained in a range of 4000-400 cm^{-1} with a summation of 64 scans and a resolution of 2 cm^{-1} using the KBr pellet technique. UV-vis absorption spectroscopy was carried out in the wavelength range of 300–700 nm by a Shimadzu UV-2600 spectrophotometer equipped with an integrating sphere. The microscopy and element dispersion of Si/PD-LDH films were determined by a scanning electron microscopy (SEM) at an acceleration voltage of 3 kV (Zeiss SUPRA 55) equipped with an energy-dispersive X-ray (EDX) spectrometer. Photoluminescent quantum yields (PLQY), fluorescence spectra, and trichromatic coordinates (CIE *x*,*y*) of LDH samples and the corresponding films were performed with an integrating sphere measurement system from Hamamatsu photonics (C9920-02G). The setup contains of a 150 W Xenon lamp, an integrating sphere coated with Spectralon (φ =3.3 inch), and a high-sensitivity CCD camera. The data were analyzed with PLQY Measurement software (U6039-05). Photoluminescence absolute quantum yield ($PLQY_{abs}$) was calculated from the internal quantum yield ($PLQY_{int}$) and absorbance (Abs) measurements according to equation:

$$PLQY_{abs} = PLQY_{int} \times Abs$$

Where $PLQY_{int}$ = number of emitted photons/number of absorbed photons, Abs = number of absorbed photons/number of incident photons (absorbance), $PLQY_{abs}$ = number of emitted photons/numbers of exciting photons. Photometric parameters were recorded using an integrating sphere with a diode array rapid analyzer system (GL Optic integrating sphere GLS 500) under a

forward current of 450 mA with the corresponding applied voltage of 3.0 V. Up to three stacked films of polysiloxane/PD-LDH were placed onto a blue LED chip to optimize the global emission.

3. RESULTS AND DISCUSSION

3.1 Structural analysis of DS-PD$_x$-LDH

An entire series of novel fluorescent inorganic-organic LDH materials is synthesized by co-intercalating four different organic PD phosphors[35-38] (the corresponding structural formulae of guest species are shown in Figures 1a) with surfactant DS acting as spacer into the interlayer of Mg_2Al-LDH. For example, Figure 1b presents the structure of DS and PTBA co-intercalated LDH matrices, in which the DS spacer is devoted to expand the LDH gallery as well as further dispersing PTBA guests in the interlayer space. A comparison of the color under daylight or UV radiation is displayed in Figure 1c. The four phosphors in solid state do not emit at all (Figure 1c(I)), as expected due to ACQ. When perylene derivative is free of substitution, its configuration is almost planar resulting in a shorter intermolecular π-π stacking as close as 0.34 nm, thus leading to a very strong ACQ.[39] It is worth noting that in spite of the substitution either at the *bay* or diimine position as performed here, that twists the planar configuration, the ACQ remains strong. This is consistent with the literature since ACQ is found efficient until a stacking of about 1 nm, and that great effort to "jacket" the entire backbone is paid by tethering with very large entities.[40,41] When dissolved in the solution with concentration as low as $5 \cdot 10^{-5}$ mol/L, the four phosphors emit because of the Brownian motion is enough to disperse the molecules (Figure 1c(II)). Interestingly the four co-intercalated LDH solids are found to strongly emit under UV radiation with an emitting color close to that observed for each phosphor in solution. As exemplified in Figure 1c(III), DS-PD$_x$-LDH samples exhibit under 365 nm UV light a bright green, yellow, orange or red emission

corresponding to DS-PTC$_x$-LDH, DS-PTBA$_x$-LDH, DS-PRSA$_x$-LDH, and DS-TSP$_x$-LDH, respectively, which is almost of the same color as that of each PD in solution. Qualitatively, the fluorescence of each phosphor is found brighter when dispersed in LDH than in solution, suggesting that an efficient dispersion is occurring within the host structure even better than the one in solution. It underlines that ACQ phenomenon of PD molecules is here strongly reduced in solid state by their confinement provided by LDH structure and their dispersion by spacer DS within the galleries. Obviously, the effectiveness in dispersing the PD molecules is limited by their quantity and the color in each series becomes darker and darker under daylight as the part of fluorophores increases, indicating that the ACQ effect also increases.

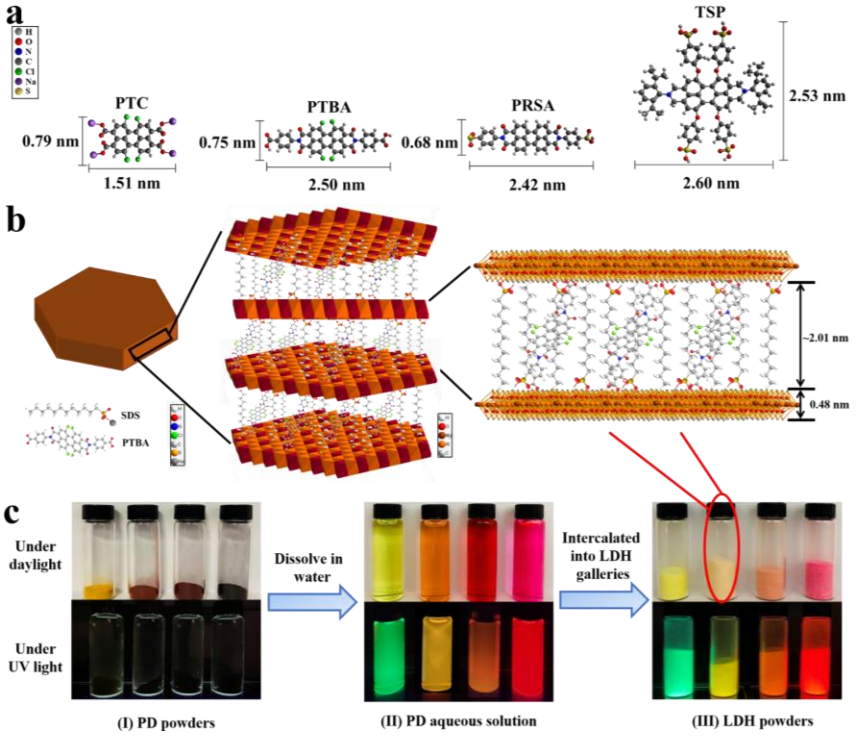

Figure 1. Schematic representation of (a) 3D chemical structures of PTC, PTBA, PRSA, and TSP and (b) co-intercalated DS-PTBA$_x$-LDH structure; (c) photographs of PD powder, PD aqueous solution (c =5·10^{-5} mol/L, pH of PTBA aqueous solution was controlled to be 9.5), and the corresponding intercalated LDH (x = 0.05 corresponding to 10^{-3} mol/L) powders under daylight and UV light (365 nm).

The XRD patterns of PD, DS-LDH and DS-$PD_{0.5}$-LDH samples are gathered in Figure 2a, and all the intercalated series shows clearly characteristic diffraction peaks, indexed to the basal reflections (003), (006), (009) and the reflection (110) typical of LDH-type structure, this in absence of the diffraction peaks of pure PD powders (Figure S1, Supporting Information). These results indicate the formation of LDH stacked structure with an intra-layer crystalline order. Besides, the mutual intermolecular organization of PD guests is disrupted when hosted into LDH, and crystallized PD molecules onto LDH platelets, here not observed, should have been removed after the successive washing steps. Evidently such low PD relative content cannot be detected by XRD, the X-Ray characterization is not relevant to address the presence of interlayer anion below 5 to 10 % by mass. Indeed, the basal spacing in the whole series is similar and equal to about 2.49 nm, which is related to the (00*l*) reflection at 3.59º, 7.09º, and 10.76º/2θ, and the interlayer spacing is about 2.01 nm taking into account of the thickness of MgAl layers (0.48 nm), this in agreement with the literature.[42] This suggests that the basal *d*-spacing of DS-PD_x-LDH is completely imposed by DS spacer located between the layers, and not by the fluorescent organic molecules owing to their very low content. As displayed in Figure 1a and b, the PTBA, PRSA, and TSP anions are slightly longer than DS backbone (2.01 nm), thus a slight tilt cannot be discarded for the phosphors to accommodate the space, as reported for similar perylene derivatives or other cumbersome organic phosphors.[43-45]

More sensitive than XRD, FT-IR is helpful to complete the characterization and the spectra of PD, DS-LDH and DS-$PD_{0.5}$-LDH samples in Figure 2b, confirming the presence of mainly the LDH host network and the DS spacer molecules all along the series. Indeed, characteristic absorption bands of Mg_2Al-LDH, DS and phosphor species are attributed as the O-H stretching vibration band around 3450 cm^{-1} assigned to the interlayer water molecules and hydroxyl of LDH

layer, the lattice vibration peak of Mg-O and Al-O (*ca*. 427 cm^{-1}) from LDH sheets, the C-H stretching vibration (*ca*. 2921 and 2847 cm^{-1}) assigned to DS spacer, and the stretching vibration of $-SO_3$ group (*ca*. 1220 and 1065 cm^{-1}) ascribed to DS guests. However, and this only for the higher phosphor content ($x \geq 0.5$), this not being detectable at the lowest levels, very low absorptions at 1658 and 1703 cm^{-1} attributed to C=O stretching vibration of the phosphors, confirm their presence in a close vicinity of Mg_2Al-LDH DS hybrid host structure.

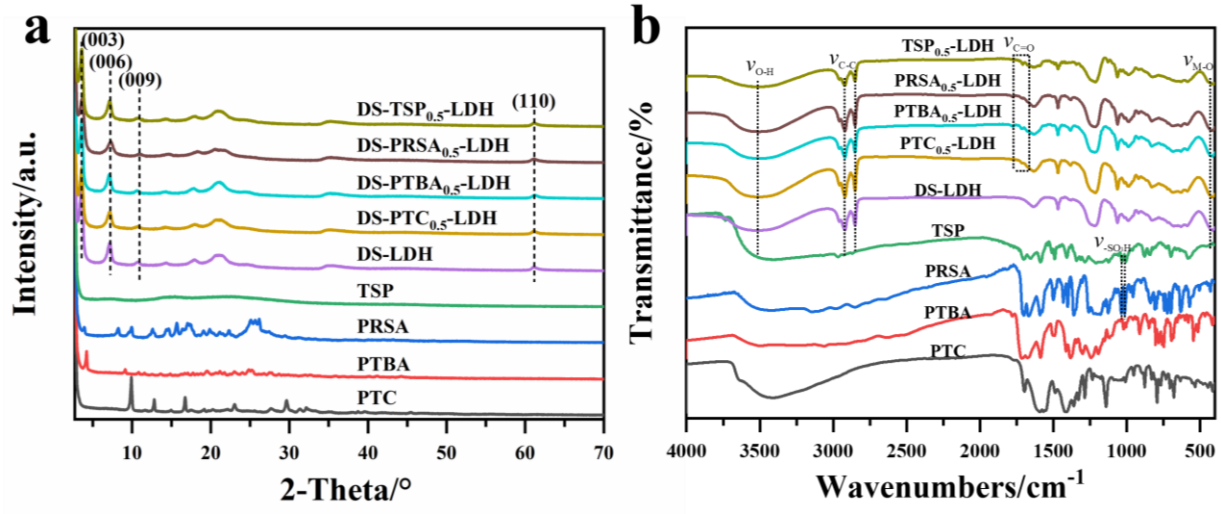

Figure 2. XRD patterns (a) and FT-IR spectra (b) of PD powders, DS-LDH, and DS-$PD_{0.5}$-LDH samples.

3.2. Photoluminescence properties of DS-PD_x-LDH

UV-vis absorption spectra of PTC, PTBA, PRSA, and TSP measured at $5 \cdot 10^{-5}$ mol/L dissolved in water are presented in Figure 3a, normalized by their maximum intensity. For perylene-based molecules, the electronic absorption displays a pronounced coupling due to the vibronic features and corresponding to $v = 0 \rightarrow v' = 0, 1, 2, 3$ transitions, where v and v' are quantum vibrational numbers of the ground and excited states, respectively.[10,46] As for all the monomers, the normal progression of Franck-Condon factors is as $A^{0\rightarrow0} > A^{0\rightarrow1} > A^{0\rightarrow2} > A^{0\rightarrow3}$. However, when the

monomers begin to self-aggregate, the 0→1 and 0→2 vibronic transitions are increased. All the synthesized phosphors present three typical absorption bands, which are found to be shifted depending on the chemical functionalization, in agreement with the literature.[47,48] *E.g.*, highly water-soluble PTC with its four carboxylate groups presents absorption maxima observed at 383 (aggregated band), 428 (aggregated band), and 446 (monomeric band) nm, assigned to vibrational modes (0→2, 0→1, 0→0) of perylene moiety. The relative intensity of 446 nm band is greater than that of 428 and 383 nm, suggesting that this phosphor is present in water mostly as monomer. The absorption maxima of PTBA generate bathochromic shifts to 462, 497, and 520 nm induced by the benzoic acid groups through imidization, and the peak of aggregates at 497 nm is stronger than the monomer (shoulder at 520 nm). This emphasizes that the aggregation is caused by the lack of solubility, while the latter is increased for PRSA in water due to its highly-polar -SO_3H groups. The absorption bands shift to 475, 504, 545 nm, and the ratio between aggregated and monomeric contribution shows that PRSA molecules aggregate in water, most probably due to the absence of Cl atoms at the *bay* region compared to PTBA, thus leading steric hindrance to decrease and π-π intermolecular stacking to interact more. TSP exhibits absorptions (453, 530, and 570 nm) more red-shifted than for PTBA and PRSA. Containing four phenoxy groups at its *bay* positions, it shows superior water solubility with sulfonyl groups substituted at the *para*-position of each phenoxy group. The strong monomeric peak at 570 nm indicates TSP mostly present as monomer in water. As previously discussed, the phosphor molecules are subjected to a diverse geometrical and chemical environment after being intercalated into the LDH layers. Such effects are followed by UV-vis spectroscopy. At a first glance, solid-state UV-vis absorption spectra of perylene-LDH compounds (Figure 3b) present broader but basically similar absorption bands with respect to the associated phosphors. Such trend could be explained by perylene-based molecules more prone to

self-aggregate in the LDH powder than in aqueous solution at concentration of $5 \cdot 10^{-5}$ mol/L. However, the interactions between perylene molecules and LDH layers as well as their dispersion by DS anions allow for a certain optimized percentages to avoid their presence too close from each other and thus to reduce their strong π-π mutual interaction.

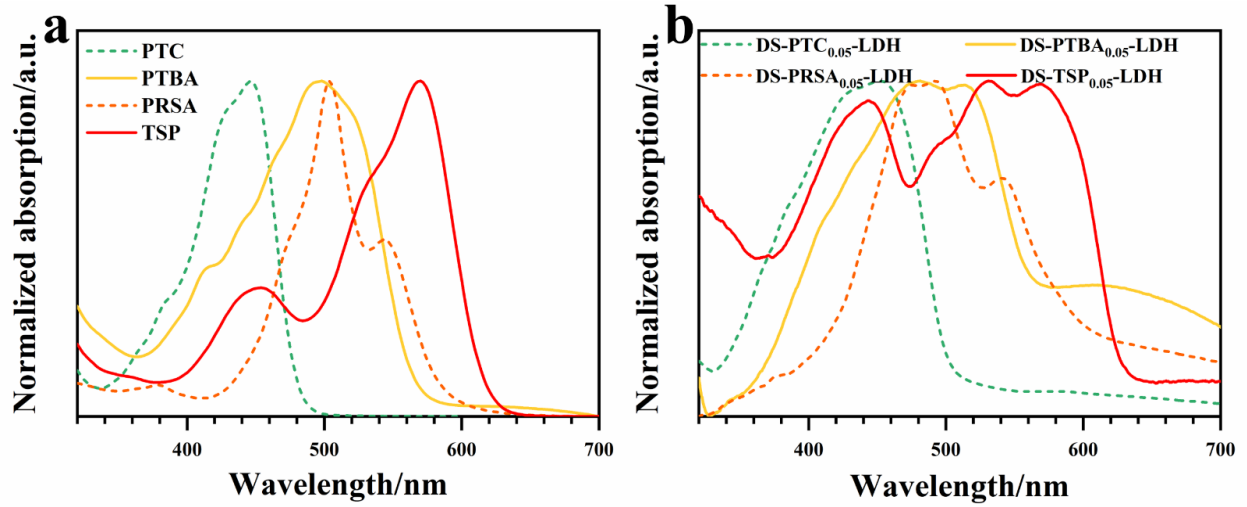

Figure 3. UV-vis absorption spectra of (a) PD aqueous solution ($c = 5 \cdot 10^{-5}$ mol/L, pH of PTBA aqueous solution was controlled to be 9.5) and (b) DS-$PD_{0.05}$-LDH samples.

Figure 4(a-c) displays the absolute photoluminescence quantum yields ($PLQY_{abs}$) as a function of the relative interleaved phosphor content for the three series. The $PLQY_{abs}$ of DS-TSP_x-LDH as a function of the TSP amount is shown in Figure S2a as the results relating to this fluorophore and its intercalation in an LDH matrix have been the subject of a dedicated study, recently published[49]. The dotted lines, in Figures 4 and S2, correspond to excitation wavelengths of common UV and blue commercial LED chips at 385, 450 and 465 nm. Figures 4(d-f) and S2c illustrate the variation in internal photoluminescence quantum yield ($PLQY_{int}$), absorbance (Abs.) and absolute photoluminescence quantum yield ($PLQY_{abs}$) as a function of the PD content within LDH under excitation at 465 nm. For each series, $PLQY_{abs}$ basically rises and then drops with increasing

content of PD, thus defining for each phosphor studied an optimal $PLQY_{abs}$. In more details and regarding DS-PTC_x-LDH samples, all the powders are excitable under both UV (385 nm) and blue (450 and 465 nm) commercial LEDs with a $PLQY_{abs}$ maximum of 18.8 % observed for PTC content of 0.1 % at λ_{exc} =455 nm (Figure 4a). Indeed, using the common excitation wavelength of 465 nm (Figure 4d), $PLQY_{int}$ increases as a function of PTC between 0.01% up to 0.1 % and then decreases sharply above. Such profile is explained by ACQ phenomenon, the dispersion effect of spacer DS efficient until of a content of interleaved phosphors of 0.1 % gradually fails when PTC molecules are closer from each other above a certain threshold of concentration. The Abs. continues to increase with increasing dye amount to reach a plateau at the higher PTC contents. The $PLQY_{abs}$ is obtained by the multiplication between $PLQY_{int}$ and Abs. (number of emitted photons/number of absorbed photons), and the maximum is obtained for a PTC concentration of 0.1 %. A similar behavior appears for DS-$PTBA_x$-LDH, DS-$PRSA_x$-LDH and DS-TSP_x-LDH series. For DS-$PTBA_x$-LDH series, a high $PLQY_{abs}$ value of 33.6 % is observed for a phosphor content of 0.01 % at λ_{exc} = 520 nm (Figure 4b, e). For DS-$PRSA_x$-LDH series, the luminescence efficiency continuously decreases with increasing amount of PRSA from 0.001 % to 0.5 %. The aggregation behavior of PRSA dye is more severe as observed in the literature,[50] and explained by its strong tendency to π-π stack each other. Hence, the maximum of $PLQY_{abs}$ corresponds to the lower amount of PRSA as low as 0.001 % for λ_{exc} = 535 nm (Figure 4c, f). For DS-TSP_x-LDH series, an optimal content of 0.1 % leads to the best $PLQY_{abs}$ of 53.8 % with an excitation wavelength of 575 nm (Figure S2(a-c)).

Having in mind to associate these materials to a commercial blue LED, their optical performance is investigated upon excitation at 465 nm. The emission spectra of DS-PD_x-LDH with different PD concentrations are displayed in Figures 4(g-i) and S2d. By increasing the ratio of PD, the

fluorescence intensity first increases and then decreases except for DS-PRSA$_x$-LDH samples whose response decreases all along. Satisfactorily, such variation agrees with that of $PLQY_{abs}$. Besides, the emission spectra illustrate the varying degrees of bathochromic-shift caused by a combination of excitonic coupling and charge transfer interactions between the π-stacked PD molecules within LDH. In the case of PTC$_x$-LDH, the emission band is wide and asymmetric from 450 up to 650 nm, with a maximum characteristic of single molecules and a broadening tail due to excimers. The emission maximum is red-shifted from 499 nm to 514 nm (green) with the PTC amount from 0.01 % to 1 %. Such small but significant red-shift of 15 nm clearly suggests an increase in fluorophores aggregation with increasing concentration. With respect to DS-PTC$_x$-LDH, DS-PTBA$_x$-LDH series produce a similar wide emission band located between 520 nm and 650 nm with a characteristic monomer peak at about 558 nm (yellow) and a large contribution above this wavelength from PTBA content as low as 0.003 %. When increasing the latter up to 0.7%, the emission peak is gradually red-shifted to 577 nm, thus showing the increase in the proportion of aggregate. In the case of DS-PRSA$_x$-LDH, the emission spectrum displays two sharp peaks centered at 549 nm (monomers) and 590 nm (aggregates) for an amount of PRSA of 0.001 %. By increasing the PRSA ratio, the monomers peak intensity drops sharply while aggregate band widens significantly with a pronounced red shift of 57 nm, giving rise to an emission of light changing from yellow to orange. For instance, the spectrum of DS-PRSA$_{0.05}$-LDH has a low intensity peak and a broad contribution at a maximum of 616 nm (orange). The latter is explained by the presence of PRSA molecules stacked in parallel while isolated PRSA centers contribute to the former. Furthermore, the emission spectra of DS-TSP$_x$-LDH also exhibit two fluorescence bands (single molecules at shorter wavelength, excimer forms at higher wavelength) covering a wide range from 550 up to 770 nm. The intensity variation between the two peaks varies as for

DS-PRSA$_x$-LDH, with a balance between the two reached at 0.3 %. It is clearly noted that the maximum of emission peak displays a bathochromic shift from 590 to 647 nm (red-shift). In addition, the fluorescence improvement of DS-TSP$_1$-LDH is of interest, as underlined recently.[45,46] According to the literature, this increase in fluorescence with abnormally high level of organic fluorophores is accountable by J-aggregates forming a non-planar structure of TSP, thus leading to a distorted π-scaffold at a higher concentration.[44] Such non-planarity increases the fluorescence by enhancing the low-energy excitonic transition. Interestingly the decrease in emission intensity as a function of PD relative content (Figure 4(g-i)) seems to be qualitatively related to the propensity of the molecules to stack each other. A same comparison is observed for the maximum of PLQY$_{abs}$ and the associated PD relative content. Indeed, the planarity between PD molecules due to the position of the substitution, *bay versus* diimide, as well as the functional group size, ranks from most planar to least as PRSA > PTC > PTBA > TSP. A same ranking is established for the emission decrease, the relative rate and the maximum of PLQY$_{abs}$. Quantitatively, the most planar molecule PRSA gives the fastest emission decay and the lowest PLQY (10 %) associated with the lowest phosphor content (0.0001 %) while the less planar TSP gives the highest PLQY$_{abs}$. This underlines that even if the host structure helps to limit the strong tendency to pile up, the molecules remain however always as sensitive to pile up between them.

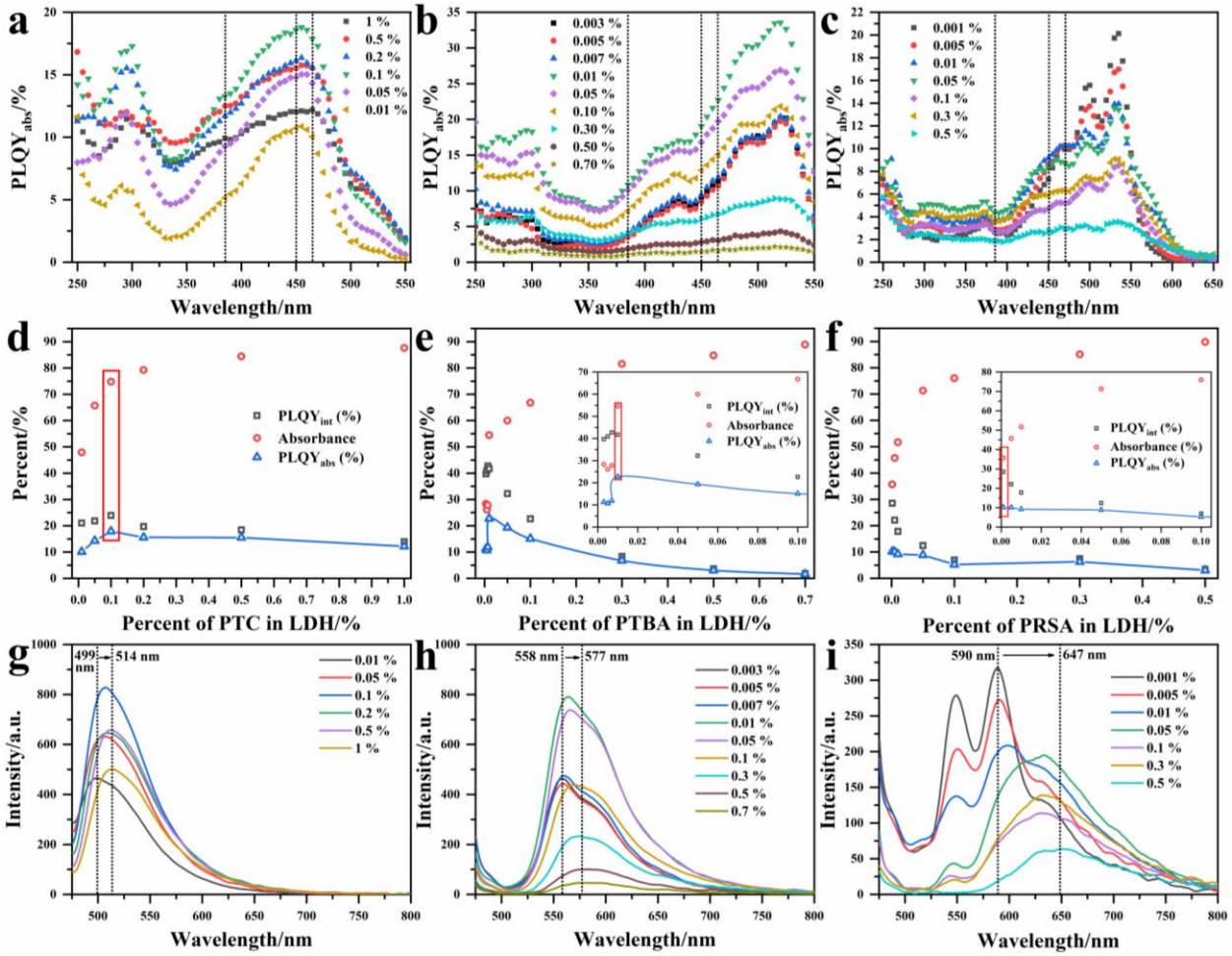

Figure 4. PLQY$_{abs}$ profile for DS-PD$_x$-LDH samples (a) DS-PTC$_x$-LDH, (b) DS-PTBA$_x$-LDH, (c) DS-PRSA$_x$-LDH as a function of phosphor content (The dotted lines correspond to the excitation wavelength at 385, 450 and 465 nm of commercial LEDs); variation in PLQY$_{int}$, Abs., and PLQY$_{abs}$ as a function of the PD content (x) (d) PTC, (e) PTBA, (f) PRSA in LDH for λ_{exc} = 465 nm (the insert is a zoom on the results recorded for low concentrations between x and 0.1% for PTBA or PRSA in LDH); emission spectra of (g) DS-PTC$_x$-LDH, (h) DS-PTBA$_x$-LDH, and (i) DS-PRSA$_x$-LDH with excitation at 465 nm.

3.3. Photoluminescence properties of silicone/PD-LDH composite films

To further evaluate the possible interest of the DS-PD$_x$-LDH powders for a LED application, four optimized compositions are selected from each series based on the best compromise between their

absolute PLQY and chromaticity coordinates to be encapsulated into polysiloxane, leading to optical-functional flexible composite films labelled hereafter Si/PD-LDH and as followed Si/PTC$_{0.1}$-LDH, Si/PTBA$_{0.05}$-LDH, Si/PRSA$_{0.05}$-LDH, and Si/TSP$_{0.1}$-LDH for each PD molecule respectively. The first three films are filled with a loading rate of 40 wt. % and the last one with several loading rate between 5 to 40 wt. %, all with a thickness of 120 ± 5 μm, and are produced according to the protocol described in the experimental part. The SEM images of the films confirm the homogenous dispersion of the LDH particles in silicone matrix, indicating a suitable compatibility between the organo-modified LDH fillers and the polymer chains (Figure S3). The optical properties of Si/PD-LDH films are assessed thoroughly by photoluminescence quantum efficiency and emission spectra, CIE color coordinates and compared to that of their counterpart DS-PD$_x$-LDH powders. The PLQY$_{abs}$ curves of Si/PD-LDH composite films with a loading rate of 40 wt.% are superimposed on those obtained for the LDH powders, showing that the dilution of LDH fillers into silicone matrix has no influence on the photoluminescence behavior (Figures 5(a-c) and S4a). From the emission spectra of the Si/PD-LDH composite films recorded under excitation at 465 nm, a slight blue-shift (towards shorter wavelengths) is observed with respect to that of LDH fillers (Figures 5(d-f) and S4c). Moreover, the ratio between monomer and excimer emission bands for polysiloxane films is slightly changed, with the contribution at longer wavelengths attributed to PD molecules aggregating less intense than for each LDH counterpart. As illustrated in Figure S4c, such slight modifications are more pronounced with a lower amount of LDH fillers within the polysiloxane. This result indicates that for each fluorophore there is an optimal concentration above which the molecules start to aggregate, thus it is necessary to define the best compromise between this phenomenon and the optical performances. Three-dimensional (3D) fluorescence plots of the film emission intensity are displayed in Figures 5(g-i) and S4d,

clearly showing that the films can be excited efficiently over a wide range of wavelengths. The CIE coordinates of the selected LDH powders and their polysiloxane films from each series plotted on a chromaticity diagram are compared in Figure 6a. All the Si/PD-LDH films obtained emit fluorescence of green, yellow, orange and red color, respectively, in accordance with the corresponding LDH powders. From direct inspection, the color of the films is visible under daylight or 365 nm ultraviolet light (Figure 6b). Afterwards, multicolor logo “ICCF” and “BUCT” were achieved by printing method with all series of Si-PD-LDH composite film, and as shown in Figure 7, they display distinctly the various fluorescent colors upon excitation at 254 nm and 365 nm UV light. It is worth highlighting that the LDH hybrid hosts suitably the phosphors as well as to be well dispersed into silicone matrix, allowing altogether to avoid optical quenching in their solid state and to provide an efficient shielding from the external environment.

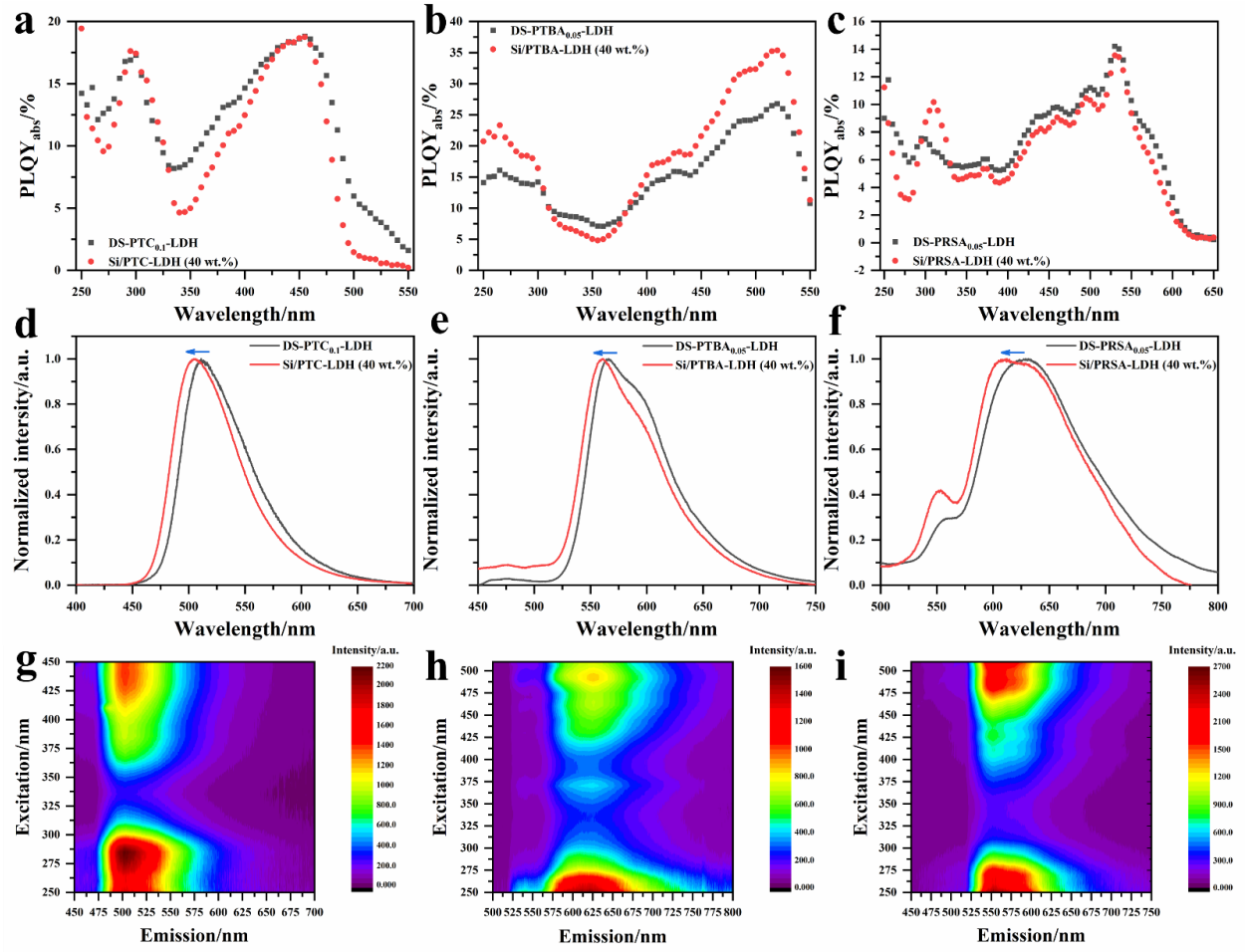

Figure 5. Evaluation of the composite films: Comparison between (a-c) $PLQY_{abs}$ and (d-f) emission spectra (λ_{exc} = 450 nm) of DS-$PTC_{0.1}$-LDH, DS-$PTBA_{0.05}$-LDH, and DS-$PRSA_{0.05}$-LDH powder (black line) and their polysiloxane composite film (40 wt.%) (red line); Three-dimensional (3D) luminescence plots (g-i) of Si/PTC-LDH, Si/PTBA-LDH, Si/PRSA-LDH film (40 wt.%).

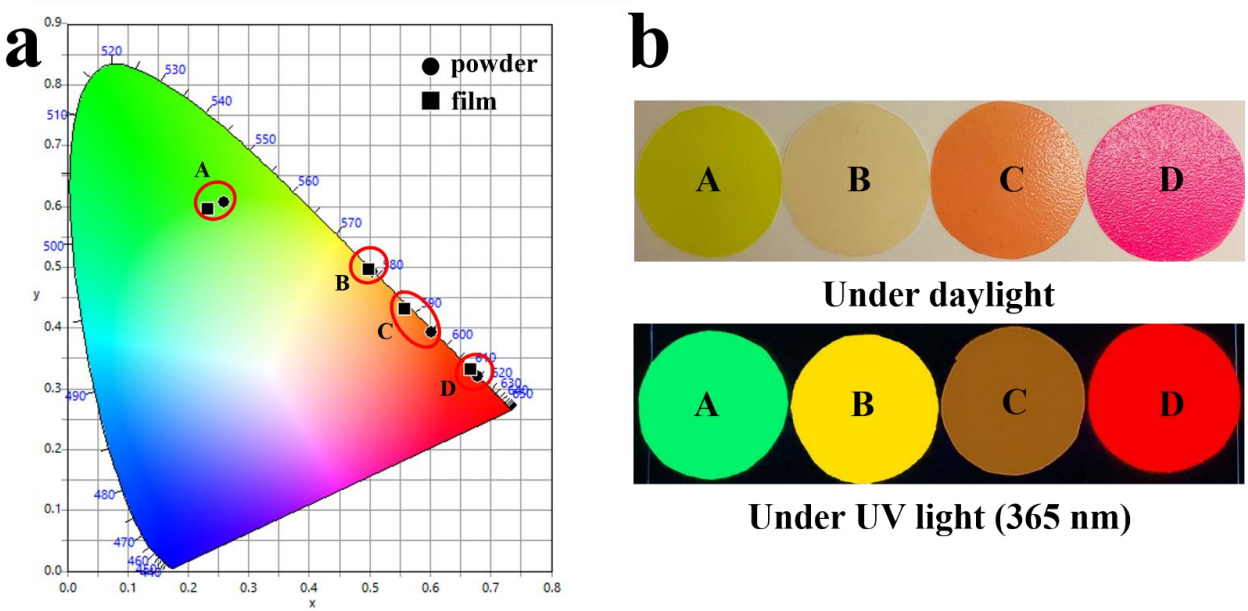

Figure 6. (a) CIE chromaticity coordinates of DS-PD$_x$-LDH powder (●) and their films (40 wt.%) (■); (b) photographs of Si/PD$_x$-LDH films (40 wt.%) under daylight and 365 nm UV light. (A: DS-PTC$_{0.1}$-LDH, B: DS-PTBA$_{0.05}$-LDH, C: DS-PRSA$_{0.05}$-LDH, D: DS-TSP$_{0.1}$-LDH).

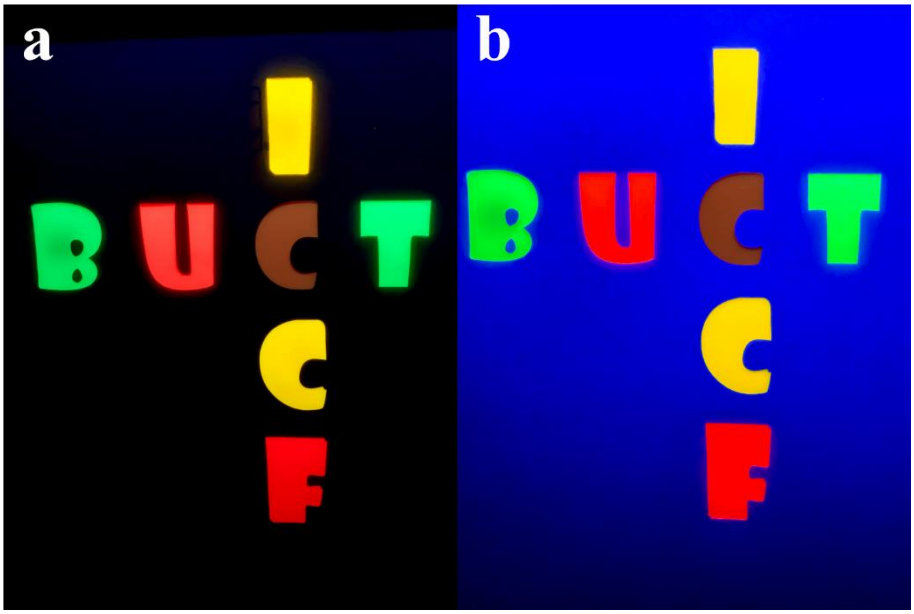

Figure 7. Printing multicolor logo "BUCT" and "ICCF" with polysiloxane/PTC$_{0.1}$-LDH (40 wt.%) (green), polysiloxane/PTBA$_{0.05}$-LDH (40 wt.%) (yellow), polysiloxane/PRSA$_{0.05}$-LDH (40 wt.%) (orange), and polysiloxane/TSP$_{0.1}$-LDH (40 wt.%) (red) (a) under 254 nm and (b)365 nm UV light.

3.4 White LED solid-state lighting applications

To confer all the optical properties of the series but in a single film, new approaches are carried out here. PRSA series is discarded since the associated $PLQY_{abs}$ is too low. The first consists in grinding together DS-$PTC_{0.1}$-LDH, DS-$PTBA_{0.05}$-conLDH and DS-$TSP_{0.1}$-LDH powders and disperse the mixture labelled after M-LDH into silicone matrix with 40 wt.% loading leading to a composite film named after Si/M-LDH (Figure 8a). The second method is to fabricate a polysiloxane composite film labelled as Si/C-LDH with a similar 40 wt.% loading but using one LDH structure C-LDH to accommodate together PTC, PTBA, TSP and DS guests (Figure S5a). The optical properties of M-LDH, C-LDH and their polysiloxane films are displayed in Figures 8 and S5. At the characteristic excitation wavelength (Figures 4 and S2) of each phosphor (455 nm, 520 nm and 575 nm), $PLQY_{abs}$ of M-LDH is about 14.9 %, 19.3 %, and 16.0 % with respect to $PTC_{0.1}$-LDH, $PTBA_{0.05}$-LDH and $TSP_{0.1}$-LDH, respectively. As usual but even more significantly, the dilution into polysiloxane promotes further the $PLQY_{abs}$ (Figure 8b). As shown in Figure 8c, the emission spectrum of M-LDH covers a range from 450 nm up to 700 nm with three relative maxima at 494 nm, 552 nm and 607 nm attributed to DS-$PTC_{0.1}$-LDH, DS-$PTBA_{0.05}$-LDH and DS-$TSP_{0.1}$-LDH, respectively. Besides, the distinct loss of emission intensity is due to the fact that the emission produced by DS-$PTC_{0.1}$-LDH is partly reabsorbed by DS-$PTBA_{0.05}$-LDH and DS-$TSP_{0.1}$-LDH and that DS-$TSP_{0.1}$-LDH moieties are also excited by the emission of DS-$PTBA_{0.05}$-LDH, thus weakening the green contribution while enhancing yellow and red. Similar observations are possible on C-LDH and its film (Figure S5b, c), underlining at first that the three phosphors are successfully present into a same LDH host, and that the interaction is more competitive between PD guests compared to M-LDH, thus leading to a stronger reabsorption phenomenon among PTC, PTBA, and TSP. The Si/M-LDH and Si/C-LDH films both exhibit CIE color

coordinates associated with yellow fluorescence, complementary to a blue chip (Figures 8d and S5d). In both approaches, these results demonstrate the presence of the three emitting phosphors in a single film. Indeed, these polysiloxane composite films should have the possibility of producing white light when combined with a blue chip.

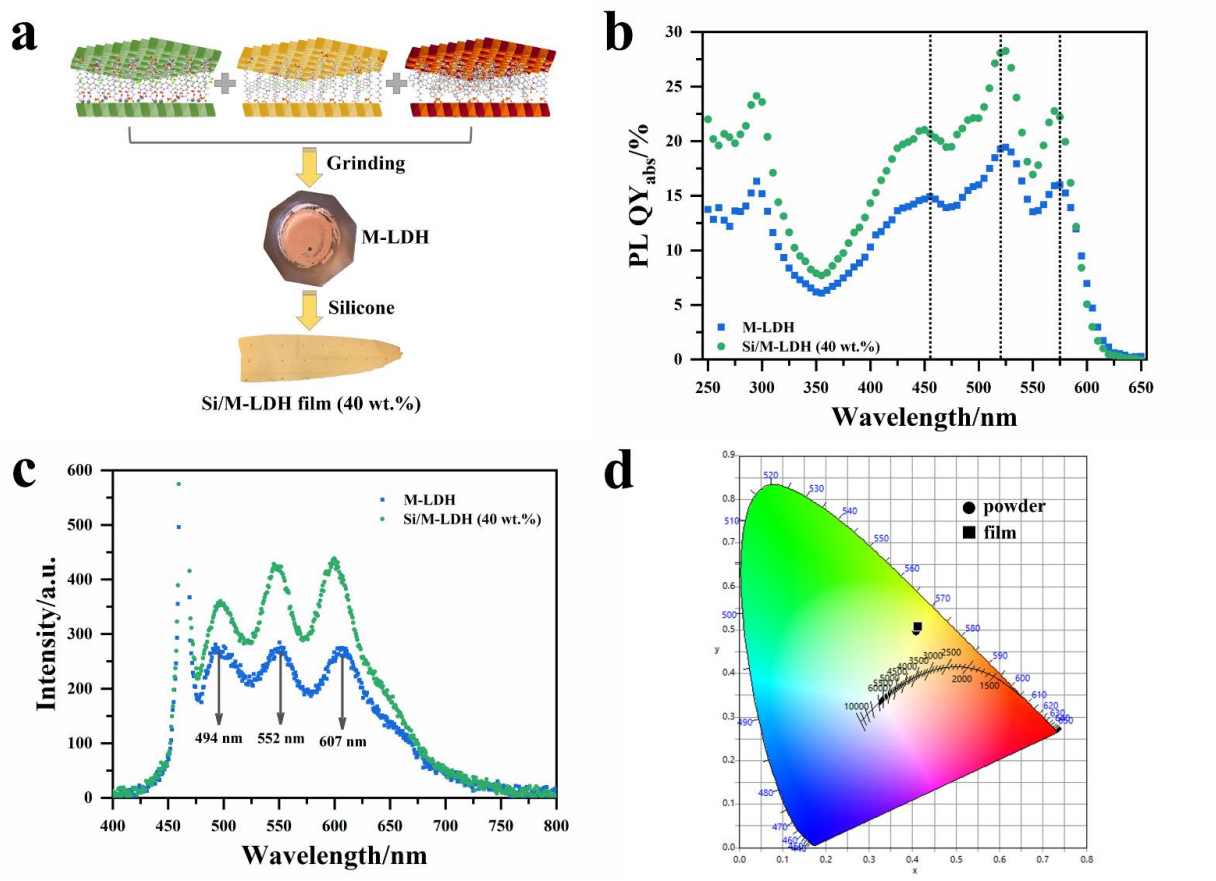

Figure 8. (a) Illustration of the fabrication of M-LDH and polysiloxane/M-LDH films by blending between $PTC_{0.1}$-LDH, $PTBA_{0.05}$-LDH, and $TSP_{0.1}$-LDH; (b) $PLQY_{abs}$, (c) emission spectra (excitation at 465 nm) and (d) CIE chromaticity coordinates of M-LDH and its corresponding polysiloxane film.

As demonstrated, the luminescence properties of Si/PD-LDH films are better than that of Si/M-LDH and Si/C-LDH as well as being more tunable due to additive effect from the stacking of films while the two other approaches are not predictive enough due to strong reabsorption. Also, to

evaluate the potential of these films to generate white light with adjustable color temperature, emitting Si/PD-LDH composite films are combined with a commercial blue LED. Experimentally, three polysiloxane films containing DS-$PTC_{0.1}$-LDH (40 wt.%), DS-$PTBA_{0.05}$-LDH (40 wt.%), and DS-$TSP_{0.1}$-LDH (5-15 wt.%) phosphors are superimposed on a 450 nm commercial LED in remote mode with the aim of achieving a warm white associated with good color rendering. To minimize the reabsorption phenomenon by Si/TSP-LDH and Si/PTBA-LDH film from the green-emitting Si/PTC-LDH film, as observed before, the stacking order is important and is as follows from top to bottom: one layer of Si/TSP-LDH, one layer of Si/PTBA-LDH, and three layers of Si/PTC-LDH on the blue chip. The emission spectra and photometric parameters of three configurations as well as a picture of the device are presented in Figure 9. For the first configuration (Figure 9a), the three Si/PD-LDH films emit a large emission from 470 up to 700 nm, and the associated intensities in green, yellow and red are comparable. The overall color is close to neutral white with the parameters CCT = 4704 K and CRI = 84.3, and the position of CIE coordinates is on the blackbody curve, further confirming that a quality white is emitted. Increasing the red-emitting response by increasing the loading of DS-$TSP_{0.1}$-LDH from 5 to 10 % in the polysiloxane film leads to a stronger contribution of red in the overall spectrum while the green contribution decreases due to the more intense reabsorption effect. The photometric parameters change to lower CCT = 3890 K and higher CRI = 91.1, with CIE coordinates still on the blackbody curve, and correspond to a neutral white light (Figure 9b). When the red-emitting phosphor (TSP) LDH filler reaches 15 wt.%, the contribution of red emission continues to be increased at the expense of the green and yellow components which are further reduced. Configuration 3 exhibits CCT = 3217 K and CRI = 84.0, and CIE coordinates in the red-emitting range, characteristic of a warmer white light (Figure 9c). Comparatively, the configuration 2 is the best which gives a neutral

white associated with excellent CRI. Such observation shows that as-made Si/PD-LDH composite films meet expectations in terms of lighting quality. Finally, perylene-core-based molecules associated to LDH materials and dispersed into polysiloxane are promising candidates to open new perspectives in eco-friendly solid state-emitting devices.

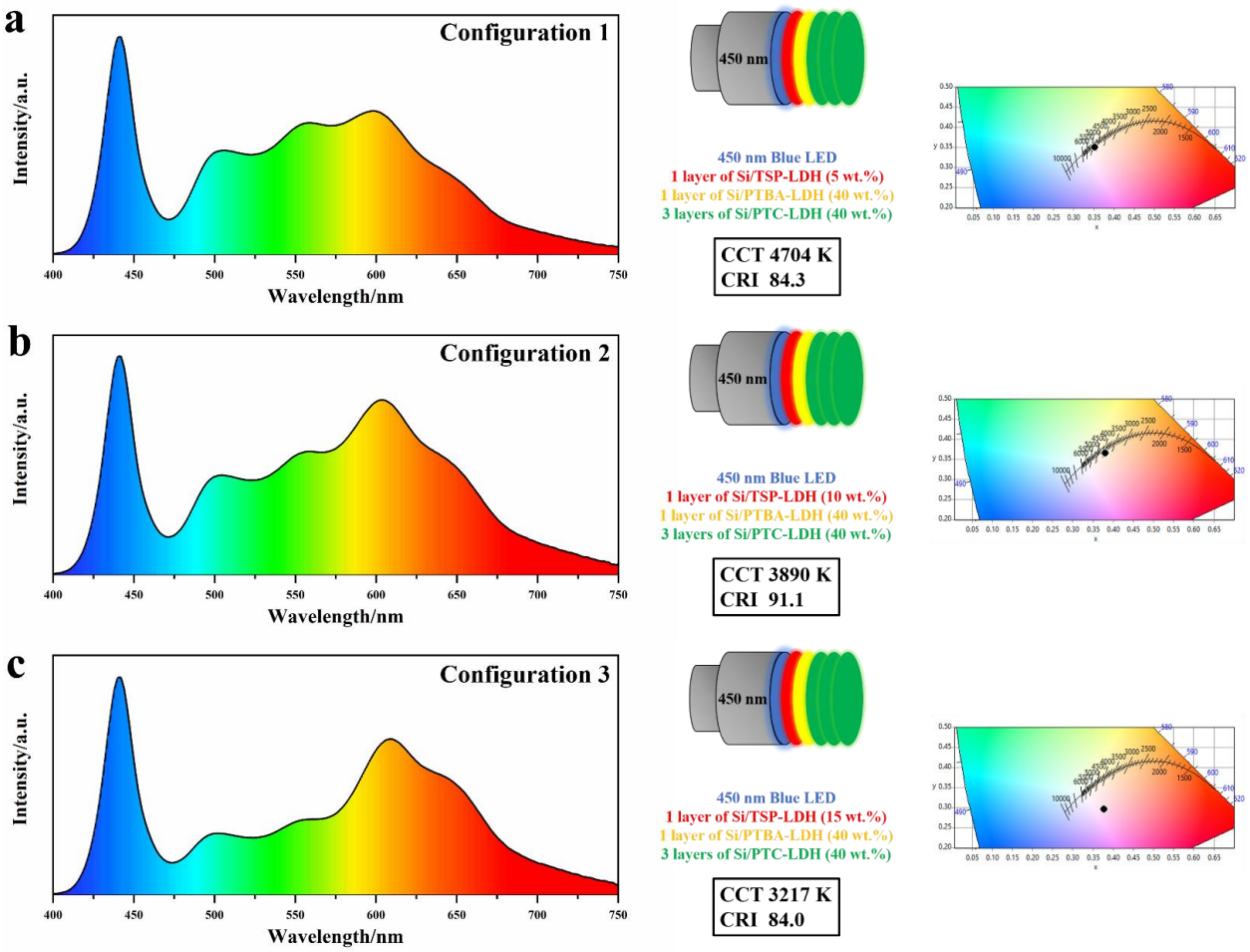

Figure 9. Emission spectrum and photometric parameters of white LED prototypes designed by combinations of a commercial blue LED with (a) configuration 1, (b) configuration 2, (c) configuration 3.

4. CONCLUSIONS

The co-intercalation of substituted perylene diamine molecules (PTC, PTBA, PRSA, and TSP) with surfactant molecules SDS into the LDH galleries leads to a series of fluorescent hybrid layered materials, while the pristine organic powders do not emit. Both bi-dimensional containment and dilution supplied by LDH and surfactant molecules, respectively, effectively limit π-π stacking between perylene-based backbones by forcing PD molecules to remain distant from each other, thus minimizing ACQ effect. However, comparisons between series show the relationship between planarity and optical behavior (maximum of PLQY and decrease in emission), emphasizing that confinement and dilution have their limits in order to contain the strong tendency of molecules to pile up together even in very small quantities. The organo-modified LDH materials loaded with PD disperse well into polysiloxane, and the resulting films show efficient luminescent properties. Taking advantage of the adjustable luminescence in emission wavelength between series, an optimized configuration mixing green-, yellow-, and red-emitting Si/PD-LDH composite films under radiation from a blue chip emits a warm white with excellent photometric performance. As demonstrated, it is possible to play with the multitude of combinations offered by the association of these DS-PD$_x$-LDH arrays with commercial blue (but also UV) diodes to produce either white light with a tunable color temperature or colored light in both cases, with a characteristic spectral profile. This highlights the value of these rare earth free materials for creating ambient light or for anti-counterfeiting marking where characteristic spectral signatures are required.

■ ASSOCIATED CONTENT

Supporting Information

The Supporting Information is available free of charge at https://pubs.acs.org/doi/XXX.

Additional experimental section: synthesis details of four fluorophores, XRD patterns of PD samples, FT-IR spectra of PD, DS-LDH, and DS-$PD_{0.5}$-LDH samples, as well as fluorescence performance data of DS-TSP_x-LDH and C-LDH samples

Notes

The authors declare no conflict of interest.

■ ACKNOWLEDGMENTS

Yixuan GUO gratefully acknowledges the support from the Joint Funds of National Natural Science Foundation of China (Grant No. ZK 20180055), and Programs for Foreign Talent (No. G2021106012L), and the financial support from China Scholarship Council (No. 202006880036).

■ REFERENCES

(1) Qin, Z.; Gao, H.; Dong, H.; Hu, W. Organic Light-Emitting Transistors Entering a New Development Stage. *Adv. Mater.* **2021,** *33*, 2007149.

(2) Salehi, A.; Fu, X.; Shin, D. H.; So, F. Recent Advances in OLED Optical Design. *Adv. Funct. Mater.* **2019,** *29*, 1808803.

(3) Zhang, X.; Dong, H.; Hu, W. Organic Semiconductor Single Crystals for Electronics and Photonics. *Adv. Mater.* **2018,** *30*, 1801048.

(4) Gao, R.; Kodaimati, M. S.; Yan, D. Recent advances in persistent luminescence based on molecular hybrid materials. *Chem. Soc. Rev.* **2021,** *50*, 5564−5589.

(5) Würthner, F.; Saha-Moller, C. R.; Fimmel, B.; Ogi, S.; Leowanawat, P.; Schmidt, D. Perylene Bisimide Dye Assemblies as Archetype Functional Supramolecular Materials. *Chem. Rev.* **2016,** *116*, 962−1052.

(6) Chen, S.; Slattum, P.; Wang, C.; Zang, L. Self-assembly of Perylene Imide Molecules into 1D Nanostructures: Methods, Morphologies, and Applications. *Chem. Rev.* **2015,** *115*, 11967−11998.

(7) Liu, Z.; Wu, Y.; Zhang, Q.; Gao, X. Non-fullerene Small Molecule Acceptors Based on Perylene Diimides. *J. Mater. Chem. A* **2016,** *4*, 17604−17622.

(8) Lü, B.; Li, P.; Li, P.; Zhang, Y.; Müllen, K.; Yin, M. Highly Fluorescent Free-Standing Films Assembled from Perylenediimide Microcrystals for Boosting Aniline Sensing. *J. Mater. Chem. C* **2020,** *8*, 1421−1426.

(9) Yang, L.; Hendsbee, A. D.; Xue, Q.; He, S.; De-Jager, C. R.; Xie, G.; Welch, G. C.; Ding, Z. Atomic Precision Graphene Model Compound for Bright Electrochemiluminescence and Organic Light-Emitting Diodes. *ACS Appl. Mater. Interfaces* **2020,** *12*, 51736−51743.

(10) Ito, F.; Kogasaka, Y.; Yamamoto, K. Fluorescence Spectral Changes of Perylene in Polymer Matrices During the Solvent Evaporation Process. *J. Phys. Chem. B* **2013,** *117*, 3675−3681.

(11) Sun, M.; Müllen, K.; Yin, M. Water-soluble Perylenediimides: Design Concepts and Biological Applications. *Chem. Soc. Rev.* **2016,** *45*, 1513−1528.

(12) Zong, L.; Zhang, H.; Li, Y.; Gong, Y.; Li, D.; Wang, J.; Wang, Z.; Xie, Y.; Han, M.; Peng, Q.; Li, X.; Dong, J.; Qian, J.; Li, Q.; Li, Z. Tunable Aggregation-induced Emission Nanoparticles by Varying Isolation Groups in Perylene Diimide Derivatives and Application in Three-Photon Fluorescence Bioimaging. *ACS Nano* **2018,** *12*, 9532−9540.

(13) Symons, H. E.; Hagemann, M. J. L.; Harniman, R. L.; Faul, C. F. J. Thionated PDI Supramolecular Polymers: Controlling Aggregation Mechanisms, Morphology and Function. *J. Mater. Chem. C* **2022,** *10*, 2828−2837.

(14) Nowak-Król, A.; Würthner, F. Progress in the Synthesis of Perylene Bisimide Dyes. *Org. Chem. Front.* **2019,** *6*, 1272−1318.

(15) Zhang, B.; Soleimaninejad, H.; Jones, D. J.; White, J. M.; Ghiggino, K. P.; Smith, T. A.; Wong, W. W. H. Highly Fluorescent Molecularly Insulated Perylene Diimides: Effect of Concentration on Photophysical Properties. *Chem. Mater.* **2017,** *29*, 8395−8403.

(16) Golshan, M.; Rostami-Tapeh-Esmail, E.; Salami-Kalajahi, M.; Roghani-Mamaqani, H., A Review on Synthesis, Photophysical Properties, and Applications of Dendrimers with Perylene Core. *Eur. Polym. J.* **2020,** *137*, 109933.

(17) Schmidt, D.; Stolte, M.; Suss, J.; Liess, A.; Stepanenko, V.; Wurthner, F. Protein-like Enwrapped Perylene Bisimide Chromophore as a Bright Microcrystalline Emitter Material. *Angew. Chem.* **2019,** *58*, 13385−13389.

(18) Faustini, M.; Nicole, L.; Ruiz-Hitzky, E.; Sanchez, C. History of Organic-Inorganic Hybrid

Materials: Prehistory, Art, Science, and Advanced Applications. *Adv. Funct. Mater.* **2018,** *28*, 1704158.

(19) Coiai, S.; Cicogna, F.; Pinna, S.; Spiniello, R.; Onor, M.; Oberhauser, W.; Coltelli, M-B.; Passaglia, E. Antibacterial LDPE-Based Nanocomposites with Salicylic and Rosmarinic Acid-Modified Layered Double Hydroxides. *Appl. Clay Sci*. **2021**, *15*, 106276.

(20) Coiai, S.; Javarone, S.; Cicogna, F.; Oberhauser, W.; Onor, M., Pucci, A., Minei, P.; lasilli, G.; Passaglia, E. Fluorescent LDPE and PLA Nanocomposites Containing Fluorescein-Modified Layered Double Hydroxides and Their ON/OFF Responsive Behavior towards Humidity. *Eur. Polym. J*. **2018**, *99*, 189-201.

(21) Yan, T.; Zhou, J.; Zhu, R. R.; Zhao, Y. R.; Xue, Z.; Jia, L.; Wang, Q.; Du, L.; Zhao, Q. H. Two-Dimensional Excitonic Metal-Organic Framework: Design, Synthesis, Regulation, and Properties. *Inorg. Chem.* **2019,** *58*, 3145−3155.

(22) Li, J.; Yuan, S.; Qin, J. S.; Huang, L.; Bose, R.; Pang, J.; Zhang, P.; Xiao, Z.; Tan, K.; Malko, A. V.; Cagin, T.; Zhou, H. C. Fluorescence Enhancement in the Solid State by Isolating Perylene Fluorophores in Metal-Organic Frameworks. *ACS Appl. Mater. Interfaces* **2020,** *12*, 26727−26732.

(23) Hou, Y.; Zhang, Z.; Lu, S.; Yuan, J.; Zhu, Q.; Chen, W. P.; Ling, S.; Li, X.; Zheng, Y. Z.; Zhu, K.; Zhang, M. Highly Emissive Perylene Diimide-Based Metallacages and Their Host-Guest Chemistry for Information Encryption. *J. Am. Chem. Soc.* **2020,** *142*, 18763−18768.

(24) Legentil, P.; Leroux, F.; Therias, S.; Boyer, D.; Chadeyron, G. Sulforhodamine B-LDH composite as a rare-earth-free red-emitting phosphor for LED lighting. *J. Mater. Chem. C* **2020,** *8*, 11906−11915.

(25) Guo, R.; Li, J.; Chen, L.; Yu, Z.; Yao, H.; Shi, K.; Li, C.; Ma, S. SDC/OS-LDH composite for highly sensitive fluorescence detection of Fe^{3+} at a much lower concentration. *Dalton Trans.* **2020,** *49*, 10413−10420.

(26) Taviot-Guého, C.; Prévot, V.; Forano, C.; Renaudin, G.; Mousty, C.; Leroux, F. Tailoring Hybrid Layered Double Hydroxides for the Development of Innovative Applications. *Adv. Funct. Mater.* **2018,** *28*, 1703868.

(27) Lv, L.; Yang, Z.; Chen, K.; Wang, C.; Xiong, Y. 2D Layered Double Hydroxides for Oxygen Evolution Reaction: From Fundamental Design to Application. *Adv. Energy Mater.* **2019,** *9*, 1803358.

(28) Jing, C.; Dong, B.; Zhang, Y. Chemical Modifications of Layered Double Hydroxides in the Supercapacitor. *Energy Environ. Sci.* **2020,** *3*, 346−379.

(29) Gao, R.; Yan, D. Layered Host-guest Long-afterglow Ultrathin Nanosheets: High-efficiency Phosphorescence Energy Transfer at 2D Confined Interface. *Chem. Sci.* **2017,** *8*, 590−599.

(30) Valleix, R.; Zhang, Q.; Boyer, D.; Boutinaud, P.; Chadeyron, G.; Feng, Y.; Okuno, H.; Reveret, F.; Hintze-Bruening, H.; Leroux, F. A First Wide-open LDH Structure Hosting InP/ZnS QDs: A New Route Toward Efficient and Photostable Red-Emitting Phosphor. *Adv. Mater.* **2021,** *33*, 2103411.

(31) Li, S.; Lu, J.; Wei, M.; Evans, D. G.; Duan, X. Tris(8-hydroxyquinoline-5-sulfonate)aluminum Intercalated Mg-Al Layered Double Hydroxide with Blue Luminescence by Hydrothermal Synthesis. *Adv. Funct. Mater.* **2010,** *20*, 2848−2856.

(32) Ma, R.; Li, R.; Liu, X.; Zhang, P.; Yang, X.; Lu, J. Restriction-induced Luminescence Enhancement in 2D Interlayer Supramolecular Infinite Solid Solution for Cell Imaging. *Adv. Opt. Mater.* **2020,** *8*, 1902019.

(33) Delgado-Pinar, E.; Costa, A. L.; Gonçalves, I. S.; Pineiro, M.; Pillinger, M.; Seixas de Melo, J. S. Tuning the Behavior of a Hydrotalcite-Supported Sulfonated Bithiophene from Aggregation-caused Quenching to Efficient Monomer Luminescence. *J. Phys. Chem. C* **2021,** *125*, 8294−8303.

(34) Li, Z.; Lu, J.; Li, S.; Qin, S.; Qin, Y. Orderly Ultrathin Films Based on Perylene/poly(N-vinyl carbazole) Assembled with Layered Double Hydroxide Nanosheets: 2D Fluorescence Resonance Energy Transfer and Reversible Fluorescence Response for Volatile Organic Compounds. *Adv. Mater.* **2012,** *24*, 6053−6057.

(35) Majumder, M.; Sheath, P.; Mardel, J. I.; Harvey, T. G. Aqueous Molecular Sieving and Strong Gas Adsorption in Highly Porous MOFs with a Facile Synthesis. *Chem. Mater.* **2012,** *24*, 4647−4652.

(36) Lü, B.; Chen, Y.; Li, P.; Wang, B.; Müllen, K.; Yin, M. Stable Radical Anions Generated from a Porous Perylenediimide Metal-organic Framework for Boosting Near-infrared Photothermal Conversion. *Nat. Commun.* **2019,** *10*, 767.

(37) Pandey, R. K.; Rana, U.; Chakraborty, C.; Moriyama, S. Higuchi, M. Proton Conductive Nanosheets Formed by Alignment of Metallo-Supramolecular Polymers. *ACS Appl. Mater. Interfaces* **2016,** *8*, 13526−13531.

(38) Kohl, C.; Weil, T.; Qu, J.; Müllen, K. Towards Highly Fluorescent and Water-soluble Perylene Dyes. *Chem. Eur. J.* **2004,** *10*, 5297−5310.

(39) Würthner, F. Perylene Bisimide Dyes as Versatile Building Blocks For Functional Supramolecular Architectures. *Chem. Commun.* **2004,** 1564.

(40) Stolte, M.; Schembri, T.; Süß, J.; Schmidt, D.; Krause, A.-M.; Vysotsky, M. O.; Würthner, F. 1-Mono- and 1,7-Disubstituted Perylene Bisimide Dyes with Voluminous Groups at Bay Positions: In Search For Highly Effective Solid-state Fluorescence Materials. *Chem. Mater.* **2020,** *32*, 6222−6236.

(41) Coleman, A. F.; Chen, M.; Zhou, J.; Shin, J. Y.; Wu, Y.; Young, R. M.; Wasielewski, M. R. Reversible Symmetry-Breaking Charge Separation in a Series of Perylenediimide Cyclophanes. *J. Phys. Chem. C* **2020,** *124*, 10408−10419.

(42) Li, C.; Liang, R.; Tian, R.; Guan, S.; Yan, D.; Luo, J.; Wei, M.; Evans, D. G.; Duan, X. A Targeted Agent with Intercalation Structure for Cancer Near-infrared Imaging and Photothermal Therapy. *RSC Adv.* **2016,** *6*, 16608−16614.

(43) Bauer, J.; Behrens, P.; Speckbacher, M.; Langhals, H. Composites of Perylene Chromophores and Layered Double Hydroxides: Direct Synthesis, Characterization, and Photo- and Chemical Stability. *Adv. Funct. Mater.* **2003,** *13*, 241.

(44) Zhang, Q.; Feng, Y.; Valleix, R.; Chadeyron, G.; Boyer, D.; Leroux, F. Co-assembled Photoactive Organic Molecules into Layered Double Hydroxide as Fluorescent Fillers for Silicone Films. *Mater. Today Commun.* **2021,** *28*, 102479.

(45) Zheng, S.; Lu, J.; Shi, J.; Duan, X. Two-dimensional Confined Electron Donor-acceptor Co-intercalated Inorganic/organic Nanocomposites: An Effective Photocatalyst for Dye Degradation. *RSC Adv.* **2017,** *7*, 2789−2795.

(46) Grande, V.; Soberats, B.; Herbst, S.; Stepanenko, V.; Wurthner, F. Hydrogen-bonded Perylene Bisimide J-aggregate Aqua Material. *Chem. Sci.* **2018,** *9*, 6904−6911.

(47) Choi, S.; Cho, K. H.; Namgoong, J. W.; Kim, J. Y.; Yoo, E. S.; Lee, W.; Jung, J. W.; Choi, J. The Synthesis and Characterisation of the Perylene Acid Dye Inks for Digital Textile Printing. *Dyes Pigm.* **2019,** *163*, 381−392.

(48) Hartnett, P. E.; Dyar, S. M.; Margulies, E. A.; Shoer, L. E.; Cook, A. W.; Eaton, S. W.; Marks, T. J.; Wasielewski, M. R. Long-lived Charge Carrier Generation in Ordered Films of a Covalent Perylenediimide-diketopyrrolopyrrole-perylenediimide Molecule. *Chem. Sci.* **2015,**

6, 402−411.

(49) Guo, Y.; Boyer, D.; Cisnetti, F.; Barros, A.; Reveret, F.; Feng, Y.; Leroux, F. Perylene Diimide Derivative Dispersed in LDH as a New Efficient Red-emitting Phosphor for LED Applications. *J. Mater. Chem. C* **2022**. DOI: 10.1039/D2TC01189A.

(50) Rana, U.; Paul, N. D.; Mondal, S.; Chakraborty, C.; Malik, S. Water Soluble Polyaniline Coated Electrode: A Simple and Nimble Electrochemical Approach for Ascorbic Acid Detection. *Synth. Met.* **2014,** *192*, 43−49.